City Research Online

City, University of London Institutional Repository

Cracks width prediction of steel-FRP bars reinforced high-strength composite concrete beams

Lei Wang[1,3], Langbo Fan[1], Feng Fu [4] [*], Zhaoping Song[3]

1 College of Civil Engineering and Architecture Engineering, Guilin University of Technology, Guilin, China
2 Guangxi Beibu Gulf Engineering Research Center for Green Marine Materials, Guilin, China
3 School of Civil Engineering, Wuhan University, Wuhan, China
4,Department of Civil Engineering, School of Mathematics, Computer Science & Engineering, City, University of London, Northampton Square, London, UK

Abstract: To study the crack development of composite steel-FRP rebar reinforced (SFCB) high strength concrete beams, a bending test of this type of beams is performed. The test shows that crack width of the SFCB beam is in between steel reinforced beam and the CFRP reinforced beam using same reinforcement ratio. The crack width of SFCB test beams is 47.9% larger than that of steel reinforced beams and 38.7% smaller than that of CFRP reinforced beams. When the steel core ratio increased from 18.37% to 32.65%, the crack width decreased by 16.5% on average before steel core yielding. After the steel core yielded, the crack width of the H-SF-3,4 beam increased at an accelerated rate. The crack width of the latter increased by 13.7% on average compared with the former. Based on test results, a new formula for calculating crack width of SFCB reinforced concrete is established, it considers the material properties of SFCB, the degradation of elastic modulus of the SFCB steel core after yielding and the compatibility of 3 different materials. It introduces a bond reduction coefficient v_i of SFCB and concrete and the compatibility coefficient s_t of the steel core and fibre layer, This formula can accurately predict the maximum crack width of SFCB reinforced concrete beams.

Keywords: SFCB; high-strength concrete beam; Normal service limit; crack width; deflection

1 Introduction

High-strength concrete has the advantages of high compressive strength, superior deformation resistance, and impressive adaptability to harsh environment construction needs. It has broad applications in tall buildings, subsea tunnels, sea-crossing bridges, and port construction [1-2]. Due to the particularity of the service environment of these projects, the corrosion of steel is more serious, as it reduces the compatibility of steel and concrete and bring serious durability problems to the structure[3-5]. Compared to steel bars, FRP bars have good corrosion resistance. However, because of the low elastic modulus and brittle failure characteristic , the FRP reinfroced concrete structure has low rigidity therefore, large deformation and large cracks under loading, showing the characteristics of brittle failure[6-10].The high-strength concrete is linear elastic before reaching the maximum stress, there are few opportunities for plastic deformation and stress redistribution; brittle failure is finally formed[11-12]. As a result, FRP reinforced high-strength concrete beams fails a very brittle manner[13-14]. In addition, the increase in the reinforcement ratio of FRP may change the failure properties from pure bending to shear failure[15]. It can be seen that FRP bars are not the most ideal substitute for ordinary steel bars.

To overcome the problems of corrosion of steel bars and the low rigidity and poor ductility of FRP bars, a new product,steel-carbon fibre composite bars (SFCBs) have gradually gained the interest of researchers. Due to the excellent mechanical properties of SFCB, the outer fibre can continue to bear the load after the steel core yields, showing a stable "secondary phase stiffness"[16]. Xiao Tongliang[17] found that the dosage of fibre has a greater impact on the strength-yield ratio of the reinforcement. Before yielding, the inner core steel and the

outer fibre can work well together After yielding, the two will produce local slippage and strain hysteresis. As a result, the backbone curve of steel-basalt composite bars was proposed. Sun Zeyang[18]pointed out that the bond strength of SFCB is approximately 94% of the corresponding ribbed steel bars .Wang et al.[19] found that the stiffness of beam decreased and the deflection and crack width increased due to the relative slippage of between the inner steel core and the fiber layers and the shrinkage of the steel core under high stress. The bending stiffness of SFCB reinforced concrete beams also increased. In addition, studies have shown that the outer fibre has a protective effect on the steel core, so that SFCB has good durability in acid, alkali and salt environments [20-23].

Existing studies have shown the excellent performance of SFCB. The combination of SFCB and high-strength concrete is expected to improve the ductility as well as good durability. Under normal conditions, concrete structures crack checking and control is particularly important. Therefore, this paper carried out the bending test of SFCB reinforced high-strength concrete beams, to investigate the influence of concrete strength and steel content on the cracks of SFCB high-strength concrete beams and studied the crack width of the beams. In addition, a new formula to predict the crack width of SFCB reinforced concrete beams is established.

2 Test Program

2.1 Test materials

The concrete strength of the beams 48 MPa and 82 MPa, the tensile strength is 3.4 MPa and 5.3 MPa, and the elastic modulus is 32.7 GPa and 38.8 GPa respectively. The detailed mixing ratio is shown in Table 1. The coarse aggregate is ordinary crushed stone with a particle size of 4.75~19 mm. The fine aggregate is ordinary natural medium sand with a fineness modulus of 2.75 and a moisture content of 5.7%. The cement adopts P.O52.5 grade ordinary Portland cement, and when preparing high-strength concrete, fly ash, mineral powder and water reducing agent are added (water reducing rate is 20%), with water reducing agent at 0.2% of the cement.

The test uses three types of SFCBs, 14 (6), 14 (8) and 16 (10), 14 mm diameter steel rebars with a diameter of and CFRP bars as the control group. 14(6) indicates that the SFCB diameter is 14 mm, the inner core diameter is 6 mm, and the apparent shape of the reinforcement is shown in Figure 1. The inner core is HRB400, and the outer layer is carbon fibre. The stirrups are made of CFRP, and the size is 70 mm×200 mm. The form of the stirrups is shown in Figure 2. Tensile specimens were made to test the mechanical properties of the bars. A thin groove of 80mm×1.5mm×3.0mm (length×width×depth) was milled in the middle of the bars. Braag grating was embedded to measure the strain of the bars and calculated according to the test results. The stress-strain curve of the bar is shown in Figure 3. The finish and mechanical properties of reinforcement are shown in Table 2.

2.2 Test Specimen

8 SFCB concrete beams, 2 reinforced concrete beams, and 2 CFRP reinforced concrete beams were tested. All beams are of the same size. The beam length is 2400 mm, the span is 2100 mm, and the cross-section size is 120 mm×250 mm. To improve the shear resistance of the test beam, the shear bending section is equipped with φ6@80 CFRP double leg stirrups, so that the test beam can be damaged by bending. The stirrups are CFRP bars with a diameter of 6mm, and the thickness of the concrete cover was 25 mm. The details of the size and reinforcement are shown in Figure 4. The letters N and H are used to indicate concrete strengths of 48 MPa and 82 MPa, respectively. The basic parameters are shown in Table 3.

2.3 Loading system and strain measurement

The loading device is shown in Figure 4, using a four-point bending method; the spacing between the loading points is 700 mm. The load increment is 3 kN, and the loading rate is 0.5 kN/s. Each increment load

was maintained for 5 minutes. After the instrument data were stable, the test data were recorded, and the load were continued until the specimen failed. Because SFCB is a composite of two materials, the strain during force is more complicated than that of a single bar. Embedding fibre grating was used to accurately measure the strain of the steel core and FRP reinforcement.

3 Test results

3.1 Crack patterns

Table 4 shows the cracking load, ultimate load and failure mode of each beam. The crack patterns and the typical failure modes are shown in Figure 5. The cracking load of the steel bar beam is 21 kN, and the initial crack height was 30% to 36% of the beam height. When loaded to 82% Pu (Pu is the ultimate load), diagonal cracks appeared in the shear-bending zone of the beam, which quickly extended to the loading point, and flexural failure finally occurred. The cracking load of the CFRP bar beam was 18 kN, and the crack extension was relatively high during cracking, reaching 60% to 68% of the beam height. When the load was increased to 36 kN, diagonal cracks appeared in the bending-shear zone, and the diagonal cracks developed to a relatively high position, reaching more than 62% of the beam height. After 45% Pu, the propagation speed of diagonal cracks was much faster than that of vertical cracks. After 75 kN, the vertical cracks basically no longer developed, the diagonal cracks continued to extend, and a small number of secondary horizontal cracks were generated near the longitudinal bars. Both test beams of the CFRP tendons suffered bending-shear failure. It can be found from the damage position that the longitudinal bars fractured, and the stirrups were broken.

The cracking load of the SFCB beam was 15-18 kN, and the initial crack height was 50% to 60% of the beam height, which is between the steel beam and the CFRP steel test beam. The initial cracks of the beams were located near the loading point of the pure bending section. When diagonal cracks appeared in the bending-shear section, the load was 31%-45%Pu. With increasing load, the inclined cracks continue to extend along the loading point. When the load was 50%~70%Pu, most of the vertical cracks develop to 80% of the beam height, and then no further development occurred. In the later stage of loading, the SFCB beam was similar to the CFRP bar test beam. Due to the large width of the diagonal crack, the force perpendicular to the longitudinal bar was generated under the dowel action, causing the diagonal crack to be developed into horizontal cracks that continue to extend along the longitudinal reinforcement. In the flexural shear zone, the concrete had insufficient bond on the longitudinal reinforcement, and the longitudinal reinforcement stress was transmitted to the end of the beam, resulting in tensile cracks. The stress loss in the anchorage zone was serious, and the slip or potential slip caused the stress increase in the shear flexural zone, and the diagonal crack rapidly penetrated through the test beam, resulting in flexural shear failure. The shear failure of the test beam occurs, but the author thinks that the shear band failure of the test beam will not affect the results or has little effect on the results. The author believes that the shear failure of the test beam may be caused by following reasons:: in the high stress stage, the longitudinal reinforcement at the end of the test beam slips due to the very large bond stress in the anchorage section of the test beam. Therefore, it can be judged that the calculation results are accurate before or near the shear failure

3.2 Crack width

The load-maximum crack width curve of each beam is shown in Figure 6. It can be seen in Figure 6(a), under the same load, the crack width of the steel reinforced beam is the smallest, and the CFRP reinforced beam has the largest crack width which is much larger than that of the steel bar beam. The crack width of the SFCB beam is between those of the steel beam and the CFRP steel test beam, which is the same conclusion drawn by Ge [24]. For example, at 54 kN, the crack width of the SFCB bar beam was 0.20~0.23 mm, while the maximum crack widths of the steel bar beam and CFRP bar beam are 0.07~0.12 mm and 0.30~0.32 mm,

respectively. During the whole loading process, the crack width of the SFCB bar beam was 47.9% larger than that of the steel bar beam and 38.7% smaller than that of the CFRP reinforced beam.

In Figure 6(b), it can be seen that before the SFCB steel core yields, the crack width of the H-SF-1,2 beam is 16.5% larger on average than that of H-SF-3,4; after the yield of steel core, the crack width of the H-SF-3,4 beam accelerates, and is gradually larger than the crack width of the H-SF-1,2 test beam. The crack width of the former is increased by 13.7% on average compared to that of the latter. The main reason is that after the steel core yields, the elastic modulus of the 14 (8) composite tendons is lower than 14 (6), and the stiffness of the H-SF-3,4 beam is lower than that of the H-SF-1,2 test beam. In addition, as the diameter (reinforcement ratio) increases, the crack width of the beam decreases, which is the same dynamic as that of the ordinary reinforced concrete test beam. The crack width of the H-SF-5 beam decreases by 31.2% and 31.8% compared with the experimental beams H-SF-1 and H-SF-3 and 4.

Figure 6(c) shows that before the SFCB steel core yields, since the concrete strength has little effect on the short-term stiffness of the concrete flexural member, the crack resistance of the two strength test beams is basically the same, and the crack width of the high-strength concrete beam is similar to the general strength concrete test beams are basically the same. After the steel core yields, After the steel core yields, the shear stress between the longitudinal reinforcement and the concrete interface is larger, and the bond strength between the high-strength concrete and the reinforcement is greater than that of the low-strength concrete, and the relative slip length is small. The crack width of the beam in the H-SF test is larger than that in the N-SF test beam.

3.3 Load-deflection curve

As shown in Figure 7, the load-deflection curves of test beams with different type of bars are significantly different. There is no significant change in the slope of the load-deflection curve of the CFRP bar beam after cracking. The SFCB beam and the steel bar beam have similar working stages, but the difference is that, after the yield of the steel bar, the deflection of the steel bar beam increases significantly, and the stiffness degradation is obvious, while the outer fiber of the SFCB beam can continue to bear the tensile force after the steel core yields, and the deflection increase is not obvious, showing the characteristics of secondary stiffness.

Under the same load, the deflection of the SFCB beam is smaller than that of the CFRP beam and larger than that of the steel test beam. For example, the mid-span deflection of H-S-1, H-C-1 and H-SF-1 in the normal service stage (0.6 MU) is 6.42 mm, 14.719 mm and 9.325 mm, respectively. The SFCB beam increases by 45% compared to the reinforced beam but decreases by 37% compared to H-C-1. It can be seen that replacing FRP bars with SFCB can effectively enhance the stiffness.

Comparing the H-SF-1 beam and H-SF-3 beam at 0.6 Mu, the mid-span deflection is 9.325 mm and 8.654 mm, respectively. When the steel content is increased from 18.37% to 32.65%, the deflection is reduced by 7.20%. The mid-span deflection increases as the ratio of fibre to steel core area increases [25-26]. The reason is that the elastic modulus of fibre materials is much smaller than that of steel bars. As the proportion of fibre increases, the stiffness of the SFCB beam is significantly reduced.

Comparing N-SF-1 and H-SF-3, it can be found that the load-deflection curves of the two beams before steel core yield are almost the same and that they develop in a similar fashion. When the load is 51 kN, the mid-span deflection is 6.220 mm and 5.885 mm, respectively. The concrete strength has little effect on deflection. After the steel core yields, the deflection decreases with increasing concrete strength under the same load. Combined with the analysis of the crack width of the test beam, this is consistent with the development of the crack width of the two test beams after the steel core yields.

3.4 Ductility analysis

According to the provisions of GB50608-2020 [27], the normal service limit state of FRP reinforced steel fiber reinforced concrete beams is defined as the corresponding state when the mid-span deflection of the test beam reaches 1/200 of the span. The observed ductility value adopts the ratio of the deflection in the ultimate state of the bearing capacity of the test beam to the deflection in the normal use state, namely:

$$\mu = \frac{\delta_u}{\delta_{ser}}$$

Where: μ is the ductility coefficient, δ_u and δ_{ser} are the deflections of the specimen at the ultimate limit state of the bearing capacity and under the limit state of normal service, respectively.

The normal service limit state of ordinary reinforced concrete specimens is the state corresponding to the yield of reinforcement. This provision is also applicable to SFCB concrete test beams with yield points. According to relevant regulations and test results, the observed ductility values of SFCB concrete test beams and CFRP reinforced concrete test beams are calculated, as shown in Table 5.

It can be seen from table 5 that except for c80-f16 (10) -2 test beams, the observed ductility values of other SFCB concrete test beams are greater than those of CFRP reinforced concrete test beams. Therefore, SFCB concrete specimens have better ductility than FRP reinforced concrete specimens.

3.5 Load-strain curve

In this test, the SFCB beam suffered bending-shear failure. Therefore, this section compares the strain of the mid-span position of the beam with that of the longitudinal bar in the shear bending centre. The load-strain curves were shown in Figure 8, and the suffixes S and C represent the strain of the steel core and the strain of the outer carbon fibre respectively.

As shown in Figure 8(a), before the bottom concrete cracks, the strain increases linearly with the load, and the reinforcement and concrete are subjected to the same force. At this time, the load is small, and the strain curves of the steel core and carbon fibre layer coincide. After concrete cracking, the tensile force is all borne by the longitudinal reinforcement, the strain increases sharply, and the slope of the curve decreases. After the yield of the steel core, the stress is mainly borne by the outer fibre layer, and the strain changes again.

Figure 8(b) shows that when the load reaches approximately 40 kN, the central strain of bending and shear changes suddenly due to the "beam turns to arch" effect. It is noteworthy that the load-strain curves of the steel core and the carbon fibre layer no longer coincide with each other after the yield of the steel core or the cracking of the concrete, and the slope deviation of the two increases with the increase of the load, indicating that the compatibility of the two is gradually weakened.

4 Crack width calculation

4.1 Existing formula for calculating crack width

In existing research, there are few studies on SFCB concrete members, and there is no formula for calculating the crack width of SFCB bending members. Designers often use the design guidelines of FRP concrete structures to design SFCB concrete structures such as: GB50608–2020[27],ISIS[28], ACI440.1R–15[29], The formulas for calculating the crack width in these specifications are shown in Table 6.

Table 2 shows that the surface forms of the SFCB and FRP bars are similar, and the difference in the elastic working stage is very small. Therefore, this paper adopts the design guide for FRP-reinforced structural concrete to calculate the crack width of the test specimen and compare it with the test results. As shown in Figure 9, GB50608–2020[27] and ISIS[28] have large calculation errors. In comparison, before the SFCB steel

core yields, ACI440.1R–15[29] can better predict the crack width of the specimen, but after the yield of the steel core, the test value is gradually greater than the calculated value, and with the increase in load, this phenomenon is increasingly obvious. The reasons are as follows: (1) The SFCB stress-strain relationship has obvious secondary stiffness. After the steel core yields, the elastic modulus decreases, and the stiffness of the beam decreases. (2)The bond between SFCB and concrete is weaker than the bond between steel and concrete. After the steel core yields, "wrapped relaxation" appears, and the bond failure is aggravated. (3)SFCB has a cooperative working relationship between the fibre layer and the steel core. After the steel core yields, the stress is greater, and the two synergistic capabilities are weakened. Therefore, it is unreasonable to directly use the formula form design guidelines for FRP reinforced concrete to calculate SFCB concrete members.

4.2 A new formula for maximum crack width

It is found from the previous section that the calculation of the crack width of the SFCB beam needs to consider the change in the elastic modulus of the SFCB steel core before and after yielding, the compatibility of the fibre layer and the steel core, and the bonding of the SFCB and the concrete must be considered.

(1) Considering the influence of the elastic modulus before and after yielding, the following relationship exists:

$$\frac{f_{sf}}{E} = \begin{cases} \dfrac{f_{sf}}{E_I} & 0 < f_{sf} \leq f_{sfy} \\ \dfrac{f_{sfy}}{E_I} + \dfrac{f_{sf} - f_{sfy}}{E_{II}} = \varepsilon_{sfy} + \dfrac{f_{sf} - f_{sfy}}{E_{II}} & f_{sfy} < f_{sf} \leq f_{sfu} \end{cases} \tag{1}$$

Where：ε_{sfy} and f_{sfy} are the strain and stress when the steel core yields, respectively

(2) Consider the compatibility of the fibre layer and steel core

From the load-strain curve, it can be seen that, before the concrete cracks, the strain coordination between the fibre layer and the steel core is better; after cracking, the synergy between the fibre layer and the steel core weakens with increasing stress level. In this paper, st represents the coefficient of cooperation between the steel core and the fibre layer. Since the bond between the steel core and the fibre layer has not yet been studied, the author, based on the experimental data in this paper, has defined it by the ratio of the strain of the steel core of the beam longitudinal reinforcement to the strain of the fibre layer. Figure 10 shows the relationship between the average strain ratio of the beam and the load. The strain of the longitudinal steel core and the fibre layer is not completely coordinated after the beam is stressed. From the load to the concrete cracking, the curve develops basically horizontally, indicating that the synergistic effect of the steel core and the fibre layer is stable at this time. Through concrete cracking to steel core yield stage, the strain ratio gradually decreases with the increase of the load, and it basically decreases in a linear trend. After the steel core yields, the strain ratio gradually stabilizes. According to the average strain ratio, s_t is 0.91~0.97 before cracking to yield, and s_t is 0.85~0.91 after yielding.

（3）Consider bond reduction

In ACI440.1R–15[29], the bonding property coefficient k_b is used to reflect the bonding ability of the longitudinal reinforcement and concrete. When the bonding performance is weaker than that of steel bars, k_b is greater than 1.0; when the bonding performance is better than steel bars, k_b is less than 1.0. The author sorted out the data of the existing SFCB pull-out test. Figure 11 shows the ratio of the bond strength of SFCB concrete to the bond strength of reinforced concrete in the literature. The bond strength of SFCB and concrete is generally 64%~97% of the bond strength of steel and concrete[22,30-34]. Therefore, k_b needs to be corrected. The correction coefficient is represented by v_i. The value of the bond strength is determined by the ratio of the bond

strength. The bond strength is mainly affected by the surface form of the reinforcement. Taking into account the difference in workmanship, the value of v_i is set to 0.70~0.85.

Combining the above factors, based on the ACI440.1R–15[28] crack width calculation formula, considering the effect of The elastic modulus before and after yielding, and introducing the reduction coefficient v_i of the bond strength between the longitudinal reinforcement and the concrete and the cooperating coefficient st of the steel core fibre layer, the calculation formula for the maximum crack of the SFCB concrete bending member can be defined as follows:

$$
w_{\max} = \begin{cases} 2\dfrac{f_{sf}}{E_I}\beta\dfrac{k_b}{s_t v_i}\sqrt{d_c{}^2 + (0.5s)^2} & 0 < f_{sf} \leq f_{sfy} \\[2ex] 2(\varepsilon_{sfy} + \dfrac{f_{sf} - f_{sfy}}{E_{II}})\beta\dfrac{k_b}{s_t v_i}\sqrt{d_c{}^2 + (0.5s)^2} & f_{sfy} < f_{sf} \leq f_{sfu} \end{cases} \tag{2}
$$

Where：$w_{\max}$ is the maximum crack width, k_b is bond-dependent coefficient, d_c is thickness of concrete cover measured from extreme tension fiber to center of bar or wire location closest thereto.

4.3 Verification of the formula

Figure 12 is the comparison between the crack width of the SFCB concrete beam calculated by the modified formula and the test results. The results show that within the normal load range, the new formula established after considering the change in elastic modulus of the SFCB steel core after yielding, the bond between SFCB and concrete, and the synergy between the steel core and the fibre layer have a good prediction ability, and the calculated value is in good   agreement with the experimental value.

5 Conclusion

1. In the test, both the SFCB concrete beam and CFRP reinforced concrete beam have bending-shear failure. The reason is that the bond of SFCB is weaker than steel rebar, leads to instantaneous slip of the longitudinal bar resulting bending-shear failure. In a follow-up study, it is suggested to increase the anchorage length and strengthen the anchorage measures.

2. The failure process of the SFCB reinforce beam is similar to that of the steel reinforced beam, which consists of elastic stage, cracking stage and failure stage. The difference is that after the SFCB steel core yields, the outer fibre can continue to bear the tensile force, showing obvious extra rigidity, The stiffness of the beam decreases as the area ratio of the fibre to the steel core increases.

3. During the entire loading process, the crack width of the SFCB concrete beam is between that of the reinforced concrete beam and the CFRP reinforced concrete test beam, which is 47.9% larger than the reinforced concrete beam and 38.7% smaller than the CFRP reinforced concrete test beam. Before the SFCB steel core yielded, the crack width decreased with the increase of steel content. When the steel content increased from 18.37% to 32.65%, the crack width decreased by 16.5% on average. After the steel core yielded, the crack width of H-SF-3,4 developed faster, and the crack width increased by 13.7% on average compared to that of the beamH-SF-1,2.

4. Combining the material properties of SFCB and considering the change in the elastic modulus of the SFCB steel core after yielding and the compatibility between materials, the bond reduction coefficient vi of SFCB and concrete and the cooperative working coefficient st of the steel core and fibre layer are introduced. According to the bond strength, the value of v_i is taken as 0.70~0.85; according to the average strain ratio, s_t is taken as 0.91~0.97 before cracking to yield, and s_t is taken as 0.85~0.91 after yielding. A new formula for calculating crack width is established, which is accurate to predict the maximum crack width of SFCB concrete test beams.

Acknowledgments

References

[1] Mahmood Aziz-Hasan,Foster Stephen-J.,Castel Arnaud. High-density geopolymer concrete for Port Kembla breakwater upgrade[J]. Construction and Building Materials, 2020.

[2] K Kuroha,S Namiki,S Kasai,et al. Application of High-strength Concrete with 60 MPa to High-rise Building[J]. Concrete Journal, 1995, 33(9): 29-39.

[3] Cai Jiangang,Dong Fenghui,Luo Zuolong. Durability of Concrete Bridge Structure under Marine Environment[J]. Journal of Coastal Research, 2018(83): 429-435.

[4] Demisa Sotiris,G Vagelis,Papadakis. Durability design process of reinforced concrete structures - Service life estimation, problems and perspectives[J]. Journal of Building Engineering, 2019, 26: 100876.

[5] Qu Fulin,Li Wengui,Dong Wenkui, et al. Durability deterioration of concrete under marine environment from material to structure: A critical review[J]. Journal of Building Engineering, 2021, 35.

[6] N F-Grace,A KSoliman,G Abdel-Sayed, et al. Behavior and Ductility of Simple and Continuous FRP Reinforced Beams[J]. Journal of Composites for Construction, 1998, 2(4): 186-194.

[7] Kassem Chakib,Farghaly Ahmed-Sabry,Benmokrane Brahim. Evaluation of Flexural Behavior and Serviceability Performance of Concrete Beams Reinforced with FRP Bars[J]. Journal of Composites for Construction, 2011, 15(5): 682-695.

[8] Zaidi Ali,Brahim Mohammed-Moulay,Mouattah Kaddou, et al. FRP Properties Effect on Numerical Deformations in FRP Bars-Reinforced Concrete Elements in Hot Zone[J]. Energy Procedia, 2017, 139(1): 798-803.

[9] Bank L.C. Progressive failure and ductility of FRP composites for construction: Review[J]. Journal of Composites for Construction, 2013, 17(3): 406-419.

[10] Issa Mohsen-A,Ovitigala Thilan,Ibrahim Mustapha-A. Serviceability and ultimate load behavior of concrete beams reinforced with basalt fiber-reinforced polymer bars[J]. ACI Structural Journal, 2016, 113(4): 757-768.

[11] Ding Guangsheng. Experimental study on mechanical properties and durability of high-strength concrete[D]. China University of Mining and Technology, 2016.

[12] Raheem Ahmed-H.-Abdel,Mahdy M,Mashaly Asmaa-A.. Mechanical and fracture mechanics properties of ultra-high-performance concrete[J]. Construction and Building Materials, 2019, 213: 561-566.

[13] M.goldston,A.remennikov,M.neaz Sheikh. Experimental investigation of the behaviour of concrete beams reinforced with GFRP bars under static and impact loading[J]. Engineering Structures, 2016, 113: 220-232.

[14] M W.Goldston,A.remennikov,M.neaz Sheikh. Flexural behaviour of GFRP reinforced high strength and ultra high strength concrete beams[J]. Construction and Building Materials, 2017, 131: 606-617.

[15] Chris G. Karayannis, Parthena-Maria K. Kosmidou and Constantin E. Chalioris.Reinforced Concrete Beams with Carbon-Fiber-Reinforced Polymer Bars—Experimental Study[J]. Fibers. 2018, 6(4), 99.

[16] Wu Gang,Wu Zhi-Shen,Luo Yun-Biao, et al. Mechanical Properties of Steel-FRP Composite Bar under Uniaxial and Cyclic Tensile Loads[J]. Journal of Materials in Civil Engineering, 2010, 22(10): 1056-1066.

[17] Xiao Tongliang, Qiu Hongxing, Sun Lanxiang. Experimental study on the tensile and compressive properties of steel-basalt fiber composite bars[J]. Journal of Southeast University (Natural Science Edition), 2014, 44(4): 805-810.

[18] Sun Zeyang, Wu Gang, Wu Zhishen, et al. Experimental study on the bond performance between steel-continuous fiber composite bar (SFCB) and concrete[J]. Earthquake Resistant Engineering, 2009, 31(1): 21-27.

[19] Lei Wang,Zhang Jiwang,Huang Changshi, et al. Comparative Study of Steel-FRP , FRP and Steel-Reinforced Coral Concrete Beams in Their Flexural Performance[J]. Materials, 2020, 13(9): 2097.

[20] Cui Y,Cheung MMS,Noruziaan B, et al. Development of Ductile Composite Reinforcement Bars for Concrete Structures[J]. Materials and Structures, 2008, 41(9).

[21] Wu G,Sun Z,Wu Z, et al. Mechanical Properties of Steel-frp Composite Bars (sfcbs) and Performance of Sfcb Reinforced Concrete Structures[J]. Advances in Structural Engineering, 2012, 15(4).

[22] Dong Zhi-Qiang,Wu Gang,Xu Yi-Qian. Bond and Flexural Behavior of Sea Sand Concrete Members Reinforced with Hybrid Steel-Composite Bars Presubjected to Wet–Dry Cycles[J]. Journal of Composites for Construction, 2016: 4016095-4016095.

[23] Fahmy MFM,Abd-elshafy ZE,Wu Z. Experimental and Numerical Evaluation of the Shear Behavior of Reinforced Concrete T-beams with Hybrid Steel-frp Stirrups[J]. Journal of Composites for Construction, 2017, 21(4).

[24] Wenjie ge,Yanming wang,Ashraf ashour, et al. Flexural performance of concrete beams reinforced with steel–FRP composite bars[J]. Archives of Civil and Mechanical Engineering, 2020, 20(2): 1-17.

[25] Safan Mohamed-A.. Flexural Behavior and Design of Steel-GFRP Reinforced Concrete Beams[J]. Materials Journal, 2013.

[26] Kara Ilker-Fatih,Ashour Ashraf-F.,Köroğlu Mehmet-Alpaslan. Flexural behavior of hybrid FRP/steel reinforced concrete beams[J]. Composite Structures, 2015: 111-121.

[27] Technical standard for fiber reinforced polymer（FRP） in construction: GB50608-2020. [S]. Beijing: China Planning Press, 2020.

[28] Network ISIS-Canada-Research. Reinforced Concrete Structures with Fifibre-Reinforced Polymers: ISIS Manual No. 3. [S]. University of Manitoba: Winnipeg, MB, USA, 2007.

[29] 440 ACI-Committee. Guide for the design and construction of structural concrete reinforced with Fiber-Reinforced Polymer (FRP) Bars[M]. Farmington Hills:American Concrete Institute, 2015.

[30] Zhang Linlin. Research on the bonding properties of steel-continuous fiber composite bars and concrete cross-section under repeated loads[D]. Southeast University, 2011.

[31] Pan Jun. Experimental study on tensile mechanical properties, durability and bonding properties of FRP-steel composite bars with concrete[D]. Shenzhen University, 2017.

[32] Gao Peiqi. Study on the mechanical properties of SFCB and its adhesion to concrete under the coupling action of chloride erosion and load[D]. Yangzhou University, 2020.

[33] Pan Jun. Experimental study on tensile mechanical properties, durability and bonding properties of FRP-steel composite bars with concrete[D]. Shenzhen University, 2017.

[34] Han Shiwen. Flexural performance and design method of FRP-reinforced steel composite bar seawater and sea sand concrete beams[D]. Harbin Institute of Technology, 2019.

Figures

Figure 1 SFCB reinforcement

Figure 2 CFRP stirrups
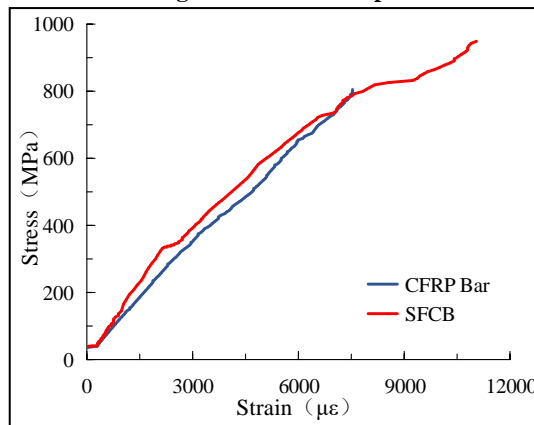
Fig.3 SFCB stress-strain curve
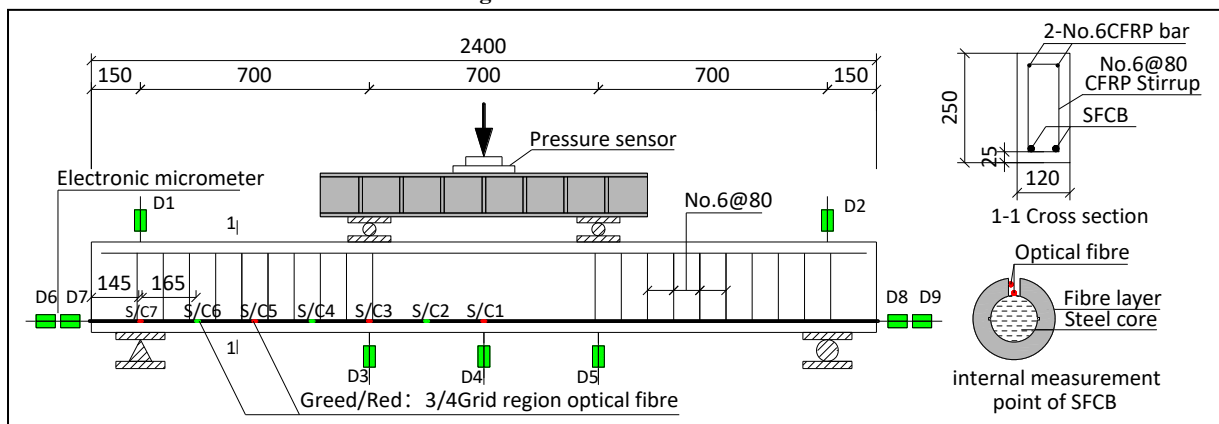
Figure 4 Test loading device and measuring point layout diagram
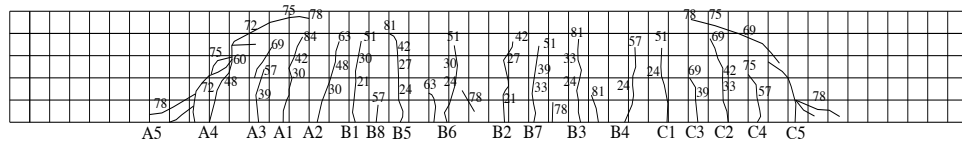
（a）H-S-1 Test beam
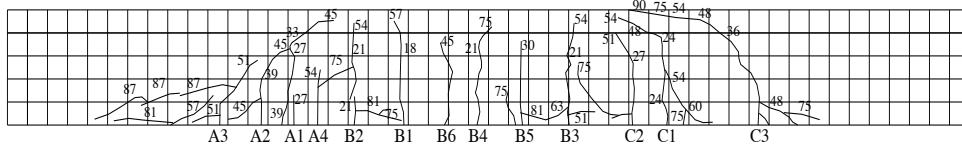
（b）H-C-2 Test beam
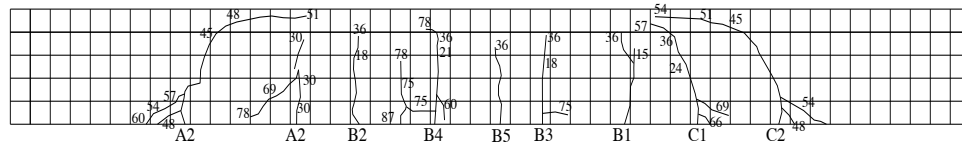
（c）H-SF-4 Test beam

Figure 5 Cracks development and failure modes
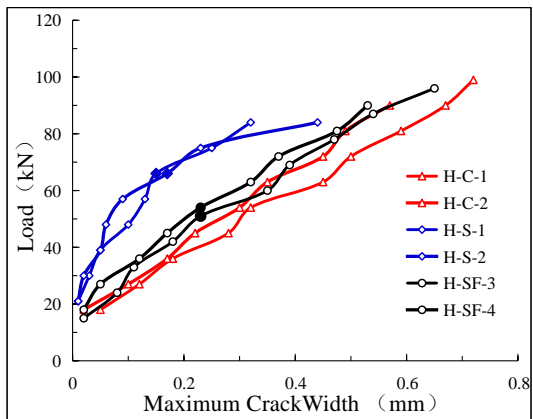
（a）Different bars
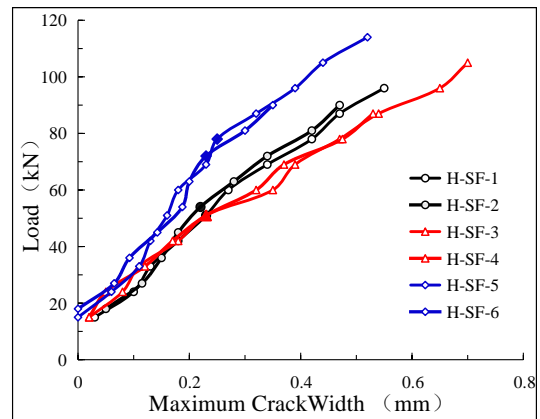
（b）Different steel content and diameter
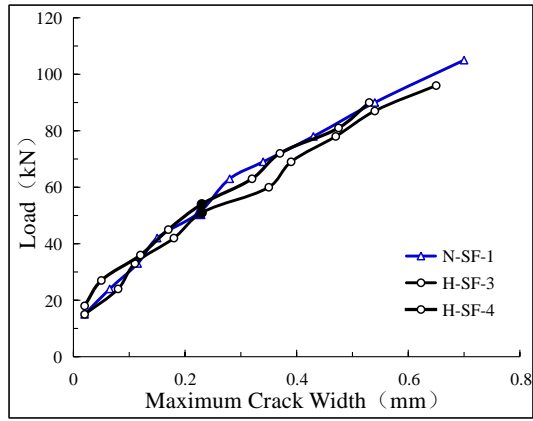
（c）Different intensities

Figure 6 Load-maximum crack width curves
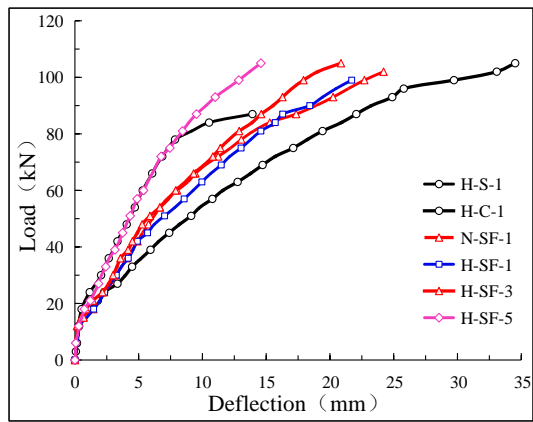
Figure 7 Load-deflection curves
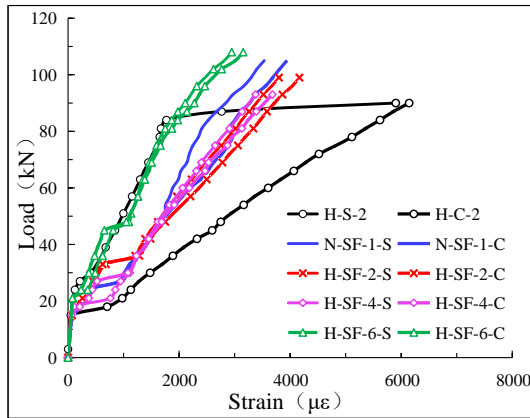
（a）Pure curve
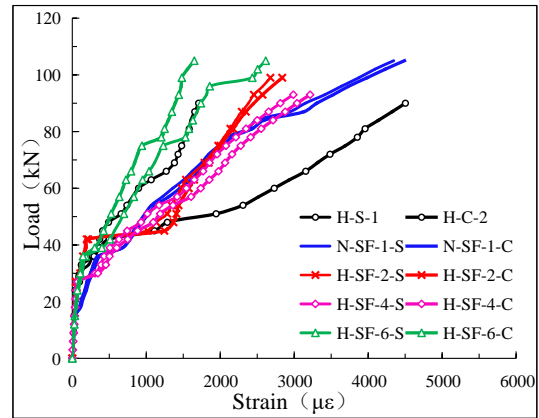
（b）Bending Shear Center

Figure 8 Load-strain curves
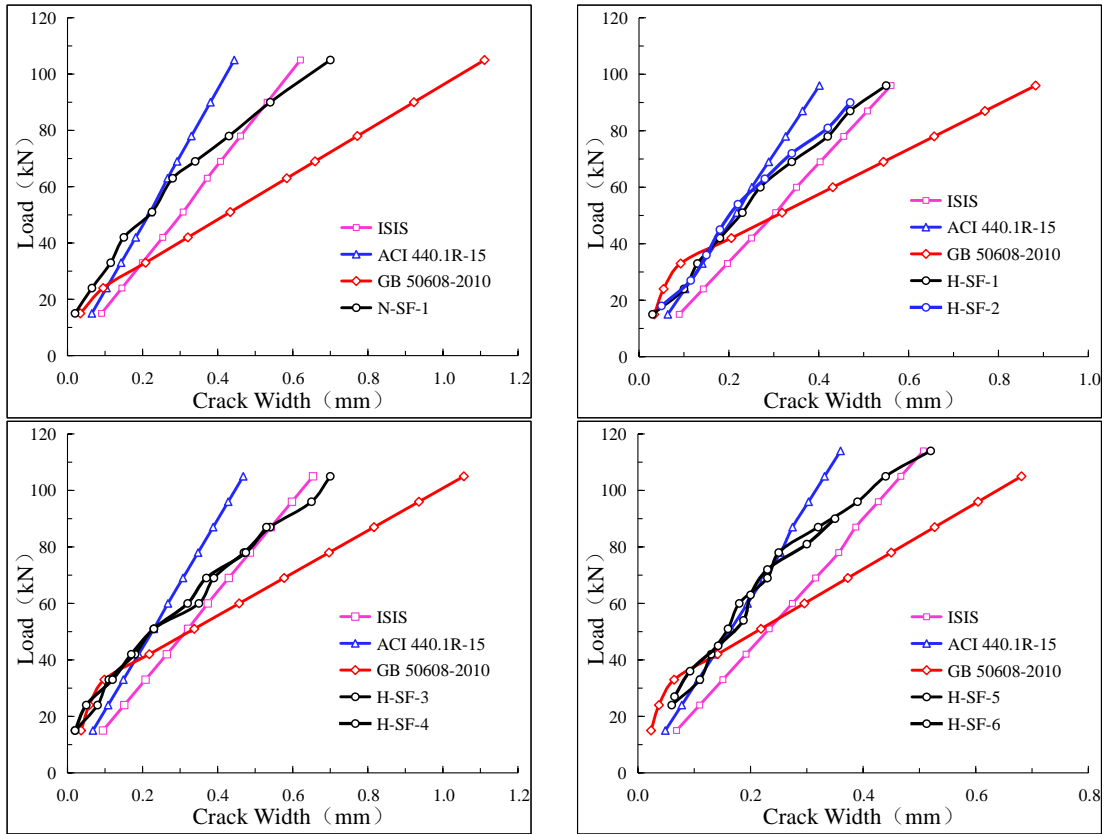
Figure 9 Standard calculated value and test value of crack width
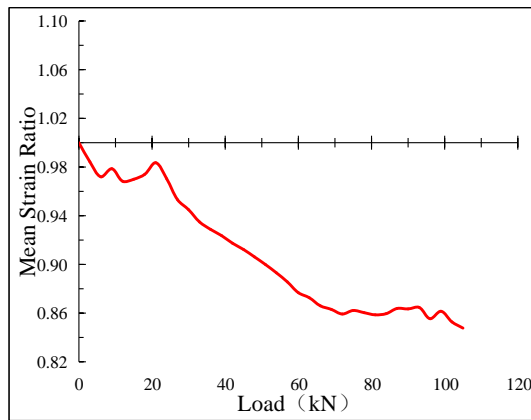
Figure 10 Load-strain ratio curve
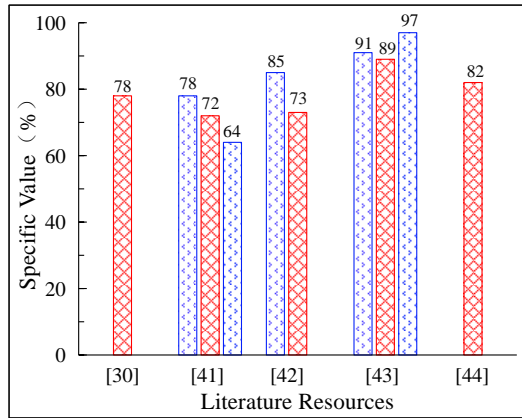
Figure 11 Bond strength
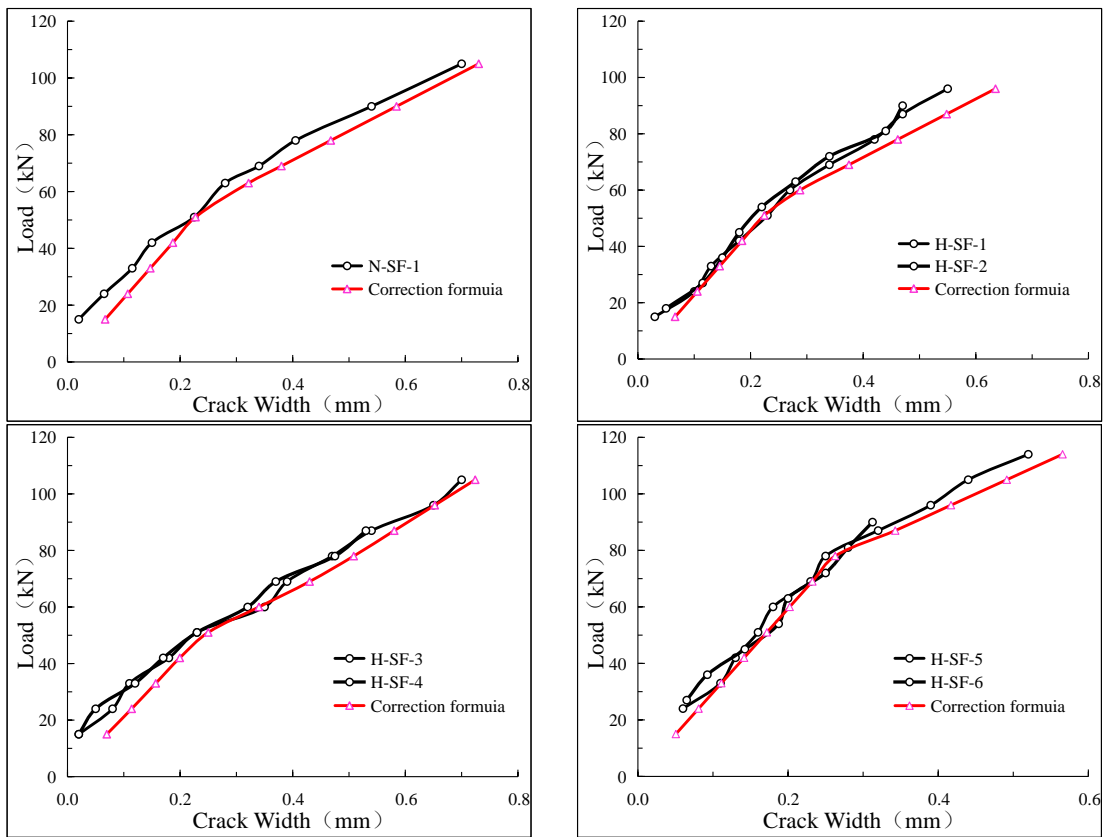
Figure 12 Calculated and experimental values of the new formula

Tables

Table 1 Detailed mix ratio

strength（MPa）	Water-cement ratio	aggregate（kg/m^3）		Cementitious material（kg/m^3）			Water reducing agent
		Pebble	Nakasago	cement	Fly ash	Mineral powder	
48	0.40	1100	720	438	/	/	/
82	0.27	1100	720	404	69	104	1.154

Table 2 Appearance characteristic parameters and mechanical properties of the reinforcement used in the test

Reinforcement type	diameter（mm）		Rib parameters（mm）			Elastic Modulus（GPa）		strength（MPa）	
	Outer diameter	Inner core	Rib height	Rib width	Rib spacing	E_I	E_{II}	Yield Strength	Ultimate strength
SFCB	14	6	0.76	10.90	13.58	141.6	104.5	292.5	1073.8
SFCB	14	8	0.55	10.41	13.37	150.2	85.7	344.8	858.4
SFCB	16	10	0.83	13.75	16.18	157.1	79.0	360.8	881.0
Steel	14	14	1.11	2.89	8.35	200.0	/	429.0	608.0
CFRP	14	/	1.22	10.28	13.84	131.6	/	/	1024.1

Note: EI and EII represent the modulus of elasticity before and after yielding, are tangent modulus.

Table 3 Basic parameters of the test beam

Beam number	Tension	CFRP frame stand bar	CFRP stirrups	Steel content	Reinforcement ratio
N-SF-1,2	2φ14（8）	2φ6	φ6@80	32.65%	1.18%
H-SF-1,2	2φ14（6）	2φ6	φ6@80	18.37%	1.18%
H-SF-3,4	2φ14（8）	2φ6	φ6@80	32.65%	1.18%
H-SF-5,6	2φ16（10）	2φ6	φ6@80	39.06%	1.54%
H-S-1,2	2φ14	2φ6	φ6@80	/	1.18%
H-C-1,2	2φ14	2φ6	φ6@80	/	1.18%

Table 4 Failure loads and failure modes

Reinforcement type	Cracking load（kN）	Ultimate load（kN）	Failure load（kN）	Maximum deflection（mm） and corresponding load（kN）	Failure mode
C30-F14（8）-1	15	48	106	24.205（102）	slip shear failure
C30-F14（8）-2	15	51	105	19.353（105）	slip shear failure
C80-F14（6）-1	15	45	114	22.404（105）	slip shear failure
C80-F14（6）-2	15	48	99	21.702（99）	slip shear failure
C80-F14（8）-1	15	48	105	20.865（105）	shear failure
C80-F14（8）-2	18	42	96	17.534（96）	shear failure
C80-F16（10）-1	15	72	126	24.611（126）	slip shear failure
C80-F16（10）-2	18	75	108.9	13.778（96）	slip shear failure
C80-G14-1	21	69	87	13.808（87）	Concrete crushed
C80-G14-2	21	69	90	10.734（84）	Concrete crushed
C80-C14-1	18	/	117	34.524（105）	shear failure
C80-C14-2	18	/	93	21.937（90）	shear failure

Table 5 The observed ductility value of the test beam

Reinforcement type	δ_u （mm）	δ_{ser} （mm）	μ
C30-F14（8）-1	24.205	5.77	4.19
C30-F14（8）-2	19.353	5.67	3.41
C80-F14（6）-1	22.404	5.3	4.23
C80-F14（6）-2	21.702	5.7	3.81
C80-F14（8）-1	20.865	4.51	4.63
C80-F14（8）-2	17.534	5.65	3.10
C80-F16（10）-1	24.611	6.76	3.64
C80-F16（10）-2	13.778	7.03	1.96
C80-C14-1	34.524	10.5	3.29
C80-C14-2	21.937	10.5	2.09

Table 6 Calculation formulas

ISIS	ACI 440.1R-15	GB50608-2010
$w = \dfrac{2.2 f_f}{E_f} \dfrac{h_2}{h_1} k_b (d_c A)^{\frac{1}{3}}$	$w = \dfrac{2 f_f}{E_f} \dfrac{h_2}{h_1} k_b \sqrt{d_c^2 + (\dfrac{s}{2})^2}$	$w = 2.1\psi \dfrac{\sigma_{fk}}{E_f}(1.9c + 0.08 \dfrac{d_{eq}}{\rho_{te}})$
$f_f = \dfrac{M_s}{A_f \cdot j \cdot d}$ 、 $j = 1 - \dfrac{\sqrt{(\rho n_f)^2 + 2\rho n_f} - \rho n_f}{3}$		$\psi = 1.1 - 0.65 \dfrac{f_{tk}}{\rho_{te}\sigma_{sk}}$ 、 $\rho_{te} = \dfrac{A_s}{A_{te}}$
$n_f = \dfrac{E_f}{E_c}$ 、 $\rho = \dfrac{A_f}{bd}$		$d_{eq} = \dfrac{\sum n_i d_i^2}{\sum n_i v_i d_i}$ 、 $\sigma = \dfrac{M}{\eta A_s h_0}$